doi.org/10.36721/PJPS.2026.39.9.261.1

3-Hydroxyflavone inhibits the cytotoxicity of oral squamous cell carcinoma cells through the AGEs/RAGE/NF-κB signaling pathway

Yuan Cong[1] and Shengzhi Wang[2]*

[1]School of Stomatology of Qingdao University, Qingdao, Shandong, 264200, China
[2]Department of Oral and Maxillofacial Surgery, The Affiliated Yantai Yuhuangding Hospital of Qingdao University, Yantai, Shandong, 264200, China

Abstract: **Background**: Advanced glycation end products (AGEs) and their receptor receptor for AGEs (RAGE) promote tumor progression via activation of the nuclear factor-kappa B (NF-κB) signaling pathway. Although 3-Hydroxyflavone exhibits anticancer properties, its role in oral squamous cell carcinoma (OSCC) and its interaction with the AGEs/RAGE/NF-κB axis remain unclear. **Objectives**: This study investigated whether 3-Hydroxyflavone inhibits OSCC by modulating miR-142-5p within the AGEs/RAGE/NF-κB axis. **Methods**: The expression of p65 and miR-142-5p was analyzed in both OSCC tissues and Tca8113 cells. TargetScan prediction and dual-luciferase reporter assays confirmed that p65 is a direct target of miR-142-5p. The effects of 3-Hydroxyflavone on OSCC cells were evaluated using MTT and colony formation assays. Additionally, immunohistochemistry was performed to assess p65 expression in tumor tissues, and Kaplan-Meier analysis was used to evaluate patient survival. **Results**: OSCC tissues showed increased p65 nuclear translocation and decreased miR-142-5p levels. The miR-142-5p directly inhibited p65. The 3-Hydroxyflavone treatment suppressed OSCC cell proliferation and colony formation by upregulating miR-142-5p and inhibiting the AGEs/RAGE/NF-κB pathway. High p65 expression correlated with poor survival, while 3-Hydroxyflavone treatment reduced p65 and improved survival. **Conclusion**: The 3-Hydroxyflavone inhibits OSCC proliferation and enhances survival by upregulating miR-142-5p, which suppresses AGEs/RAGE/NF-κB signaling, suggesting a novel therapeutic strategy.

Keywords: 3-Hydroxyflavone; AGEs/RAGE/NF-κB; Oral squamous cell carcinoma; MiR-142-5p; Mechanism

Submitted on 13-08-2025 – Revised on 27-02-2026 – Accepted on 16-03-2026

INTRODUCTION

Oral squamous cell carcinoma (OSCC) represents a major global health concern due to its high morbidity and mortality rates. As a predominant form of oral and oropharyngeal cancer, OSCC severely impacts patient quality of life (Tan *et al*., 2023; Contrera *et al*., 2025). According to the American Cancer Society (ACS), the average age at diagnosis is 62 years, with only a quarter of cases detected at early stages. Notably, males are more susceptible to OSCC than females (Keam *et al*., 2021). Although conventional therapies, including surgery, radiotherapy, and chemotherapy, have advanced, the five-year survival rate remains disappointingly low at approximately 50-55% (Tarle and Luksic, 2024). Consequently, the identification of novel therapeutic targets and the development of effective pharmacological agents are urgently needed.

Advanced glycation end products (AGEs), formed through non-enzymatic glycation and oxidation of proteins and lipids, accumulate in tissues during aging and in diabetic conditions. The receptor for AGEs (RAGE), a transmembrane protein of the immunoglobulin superfamily, functions as a multi-ligand signaling receptor (Dong *et al*., 2022). AGE-RAGE binding initiates downstream signaling, notably activating nuclear factor-κB (NF-κB) and upregulating NF-κB-dependent cytokines such as vascular cell adhesion molecule (VCAM) and intercellular adhesion molecule-1 (ICAM-1) (Li *et al*., 2023). Elevated RAGE expression correlates with the pathogenesis of various chronic diseases, and the AGEs/RAGE/NF-κB axis is critically involved in conditions such as diabetes and Alzheimer's disease, suggesting its potential relevance in oncogenesis. In breast cancer, for instance, increased serum AGEs activate the RAGE//Toll-like receptor 4 (TLR4)/myeloid differentiation primary response 88 (MyD88) pathway, promoting inhibitor of kappa B alpha (Iκ Bα) degradation, NF-κB p65 nuclear translocation, and subsequent upregulation of effector molecules such as matrix metalloproteinase-9 (MMP9), ultimately enhancing cancer cell migration and invasion (Pan *et al*., 2022). These findings suggest that aberrant AGEs/RAGE signaling constitutes a key driver of malignant progression.

NF-κB plays a pivotal role in tumorigenesis by regulating the transcription of target genes upon activation. The p65 subunit (also known as RelA) is a central component of the NF-κB family, with its activity modulated by diverse post-translational modifications, particularly phosphorylation (Liu *et al*., 2024). Aberrant p65 expression or function has been linked to the progression of multiple cancers. For example, epidermal growth factor receptor (EGFR) activation can induce abnormal signaling through the AGEs/RAGE/NF-κB pathway. Furthermore, p65

**Corresponding author:* e-mail: wangsz961@126.com

expression is lost in approximately 50% of lung cancer specimens, implying that epigenetic mechanisms may contribute to this silencing (Hong *et al*., 2022; Feng *et al*., 2022).

Traditional Chinese medicine represents a valuable source of therapeutic compounds, with many of its principles yet to be fully elucidated (Gan *et al*., 2023). The investigation of bioactive constituents, such as 3-Hydroxyflavone, is crucial for developing readily applicable and globally acceptable treatment approaches, thereby advancing traditional medicine (Zhao *et al*., 2023). 3-Hydroxyflavone, employed in both Chinese and European traditional practices, has an established safety profile, being approved under China's National Food Safety Standards and granted Generally Recognized as Safe (GRAS) status by the U.S. FDA. These compounds exhibit diverse biological activities, including heat-clearing, detoxification and hepatoprotective effects and have demonstrated clinical potential in cancer therap (Rajesh and Sangeetha, 2024). Nevertheless, research on the antitumor mechanisms of 3-Hydroxyflavone, especially concerning OSCC, remains limited, warranting further exploration (Ayoolu *et al*., 2022). MicroRNAs (miRNAs) have emerged as critical regulators of disease pathogenesis, particularly in cancer development (Lin *et al*., 2020). Notably, miR-142-5p has been implicated in modulating NF-κB-associated signaling (Li *et al*., 2021). However, whether 3-Hydroxyflavone exerts inhibitory effects on OSCC by influencing miR-142-5p to modulate the AGEs/RAGE/NF-κB pathway remains unknown.

Based on these considerations, this study aimed to determine whether 3-Hydroxyflavone inhibits OSCC cell proliferation and enhances patient outcomes by regulating the miR-142-5p/AGEs/RAGE/NF-κB axis, thereby identifying novel therapeutic targets and strategies for OSCC management.

MATERIALS AND METHODS

Collection and processing of patient samples

This study enrolled 83 patients with primary oral squamous cell carcinoma (OSCC) who underwent curative surgical resection at the Department of Oral and Maxillofacial Surgery, The Affiliated Yantai Yuhuangding Hospital of Qingdao University between November 2017 and November 2019.

Inclusion criteria were: (1) histopathologically confirmed primary OSCC; (2) no prior radiotherapy, chemotherapy, targeted therapy, immunotherapy, or traditional Chinese medicine treatment for OSCC; (3) availability of sufficient tumor and matched adjacent normal tissues (>2 cm from tumor margin) for subsequent experiments; (4) complete clinical records; and (5) signed written informed consent.
Exclusion criteria were: (1) previous antitumor treatment; (2) recurrent or metastatic OSCC; (3) concurrent other active malignancies; (4) uncontrolled severe systemic diseases (e.g., cardiovascular disease, hepatic or renal insufficiency, uncontrolled diabetes mellitus); (5) autoimmune or chronic inflammatory diseases; (6) pregnancy or lactation; or (7) incomplete clinical or follow-up data. Among the 83 tumor tissue samples, 25 with high viability and sufficient volume ($\geqslant$0.5 cm^3) were selected for primary cell culture, while the remaining samples were used for protein/RNA extraction and histological analysis. This study was approved by the Ethics Committee of The Affiliated Yantai Yuhuangding Hospital of Qingdao University (Approval Number: QD2025089).

Cell culture

Cell lines and primary cells: The human OSCC cell line Tca8113 (obtained from the Shanghai Institute of Life Sciences) and primary OSCC cells were used. Primary OSCC cells were isolated as follows: fresh tumor tissues were minced and digested with collagenase IV (1 mg/mL; Sigma-Aldrich, St. Louis, MO, USA) at 37°C for 1 hour. The resulting cell suspension was filtered through a 200-mesh sieve and collected cells were resuspended in Dulbecco's Modified Eagle Medium/Nutrient Mixture F-12 (DMEM/F12) supplemented with 10% fetal bovine serum (FBS) and 1% penicillin/streptomycin. Cells were cultured in a humidified incubator at 37°C with 5% CO_2 (Ai *et al*., 2021).

For normal controls, matched normal oral mucosal tissues were digested with trypsin-EDTA and cultured in keratinocyte serum-free medium. All cells were maintained in DMEM/F12 medium containing 10% FBS at 37°C under 5% CO_2 and passaged every 2-3 days.

Main reagents and instruments

Drugs: 3-Hydroxyflavone (CAS: 577-85-5, purity ≥98%, purchased from BIOFOUNT) was dissolved in dimethyl sulfoxide (DMSO) to prepare a 100 mM stock solution, stored at -20°C and diluted to working concentrations with complete medium before use. Reagents: RAGE inhibitor (FPS-ZM1); rabbit anti-p65 antibody (#8242, CST); rabbit anti-phosphorylated p65 (p-p65, Ser536) antibody (#3033, CST); mouse anti-RAGE antibody (sc-80652, Santa Cruz); rabbit anti-Glyceraldehyde-3-phosphate dehydrogenase (GAPDH) antibody (#5174, CST); HRP-labeled goat anti-rabbit/anti-mouse secondary antibodies (#7074/#7076, CST). 3-(4,5-dimethylthiazol-2-yl)-2,5-diphenyltetrazolium bromide (MTT) (Sigma-Aldrich, SP1080); Lipofectamine 3000 (Thermo Fisher, L3000001); Dual-Luciferase Reporter Assay Kit (Beijing Omni-Gene, 210913). Instruments: Multi-mode microplate reader (Cytation 3, BioTek Instruments, Winooski, VT, USA); Real-time polymerase chain reaction (PCR) instrument (PIKOREAL 96, Thermo Fisher Scientific, Waltham, MA, USA); Chemiluminescence imaging system (GS-600UV, GeneScript, Piscataway, NJ, USA); Fluorescence microscope (IX83, Olympus, Tokyo, Japan); Microtome (RM2255, Leica Biosystems, Nussloch, Germany).

MTT assay

Tca8113 cells were seeded in 96-well plates at a density of 2×10^3 cells per well. After 24 hours of incubation to allow attachment, experimental groups were treated with 3-hydroxyflavone at 20 μM, while control groups received an equal volume of dimethyl sulfoxide (DMSO) vehicle. After 24, 48, and 72 hours of treatment, 20 μL of MTT solution (5 mg/mL) was added to each well, and the plates were incubated at 37°C for 4 hours. The supernatant was carefully aspirated and 150 μL of DMSO was added to each well to dissolve the formazan crystals. Absorbance was measured at 490 nm using a microplate reader. Each treatment group contained six replicate wells and the experiment was performed in triplicate (Zou *et al*., 2022).

Reverse transcription quantitative PCR (RT-qPCR)

Total RNA was extracted and treated with 10 U DNase I (Roche) and RNase inhibitor (Roche) at 37°C for 20 minutes. After heat inactivation, cDNA was synthesized and amplified using gene-specific primers, with GAPDH serving as an internal control for normalization. Relative gene expression was calculated using the $2^{-\Delta\Delta Ct}$ method (Ai *et al*., 2021). The primer sequences are listed in table 1.

Western blotting analysis

Total protein was extracted from cells or tissues using radioimmunoprecipitation assay (RIPA) lysis buffer supplemented with 1 mM phenylmethylsulfonyl fluoride (PMSF) and protease inhibitors. Protein concentration was determined using a bicinchoninic acid (BCA) assay. Equal amounts of protein (30 μg per lane) were separated by 10% sodium dodecyl sulfate-polyacrylamide gel electrophoresis (SDS-PAGE) and transferred to polyvinylidene difluoride (PVDF) membranes. Membranes were blocked with Tris-buffered saline containing 0.1% Tween-20 (TBST) and 5% skim milk for 1 hour at room temperature, then incubated with primary antibodies overnight at 4°C. After washing with TBST, membranes were incubated with corresponding horseradish peroxidase (HRP)-conjugated secondary antibodies for 1 hour at room temperature. Protein bands were visualized using enhanced chemiluminescence (ECL) substrate and band intensity was quantified using Image Lab software (Bio-Rad). GAPDH served as the loading control (Li , 2022).

Cell transfection

Tca8113 cells were detached with 0.25% trypsin and seeded into 6-well plates. After 18 hours, the medium was replaced with serum-free DMEM/F12. For transfection, 5 nmol of small interfering RNA (siRNA) was diluted in 250 μL of DMEM/F12 medium. In parallel, 5 μL of Lipofectamine 3000 was diluted in 250 μL of DMEM/F12 medium. Both mixtures were incubated at room temperature for 5 minutes. The diluted siRNA was then combined with the diluted Lipofectamine 3000 and incubated for an additional 25 minutes at room temperature. The transfection complex was added dropwise to the Tca8113 cell cultures. After 6 hours, the medium was replaced with fresh DMEM/F12 containing 10% FBS and cells were cultured for an additional 48 hours (Shan *et al*., 2023).

Dual luciferase reporter gene assay

Cells were co-transfected with the pEZX-MT06 reporter vector containing the 3'-untranslated region (3'-UTR) of p65, along with either miR-142-5p mimic or scrambled miRNA control (miR-control) (Li, 2022).

Immunofluorescence assay

Cell slides were fixed with 4% paraformaldehyde for 15 minutes, permeabilized with 0.1% Triton X-100 for 10 minutes, and blocked with 5% Bovine Serum Albumin (BSA) for 30 minutes. Subsequently, they were incubated overnight at 4°C with a primary antibody against p65 (1:200 dilution), followed by incubation with an Alexa Fluor 488-labeled secondary antibody (1:500 dilution) at room temperature for 1 hour in the dark. Nuclei were stained with 4',6-Diamidino-2-Phenylindole (DAPI) for 5 minutes. After sealing, the slides were observed under a fluorescence microscope (Pai *et al*., 2021).

Immunohistochemical staining

Paraffin sections were deparaffinized, rehydrated, and subjected to antigen retrieval. Endogenous peroxidase activity was blocked using 3% hydrogen peroxide (H_2O_2). The sections were then incubated with p65 primary antibody (1:300 dilution) at 37°C for 1 hour, followed by incubation with an HRP-labeled secondary antibody at room temperature for 30 minutes. Staining was developed with 3,3'-diaminobenzidine (DAB) and nuclei were counterstained with hematoxylin. After dehydration, the sections were mounted. Two pathologists independently scored the slides in a blinded manner based on staining intensity (0–3 points) and the percentage of positive cells (0–4 points). The product of these two scores yielded a composite score ranging from 0 to 12. A composite score ≤ 4 was classified as the p65 low-expression group, while a score > 4 was classified as the p65 high-expression group. If the difference between the scores assigned by the two pathologists exceeded 2 points, a third senior pathologist conducted a re-evaluation to reach a final decision (Pai *et al*., 2021).

Statistical analysis

All data were expressed as the mean ± standard deviation (SD). The difference between the two groups was compared using a Student's t-test. Comparisons among multiple groups were performed using one-way analysis of variance (ANOVA) followed by Tukey's post hoc test. Survival analysis was conducted using the Kaplan-Meier method with the log-rank test. P <0.05 refers to a significant difference. All analyses were performed using GraphPad Prism 8.0 software.

Table 1: Real-time PCR primers and primer sequences.

Primer		Primer sequence (5'→3')
PFKFB3	*Forward primer*	GATCTGGGTGCCCGTCGATCACCG
	Reverse primer	CAGTTGAGGTAGCGAGTCAGCTTC
P65	*Forward primer*	GGCTACACAGGACCAGGAACAG
	Reverse primer	AGGAACTATGGATACTGCGGTCTG
GAPDH	*Forward primer*	AGGTCGGTGTGAACGGATTTG
	Reverse primer	TGTAGACCATGTAGTTGAGGTCA

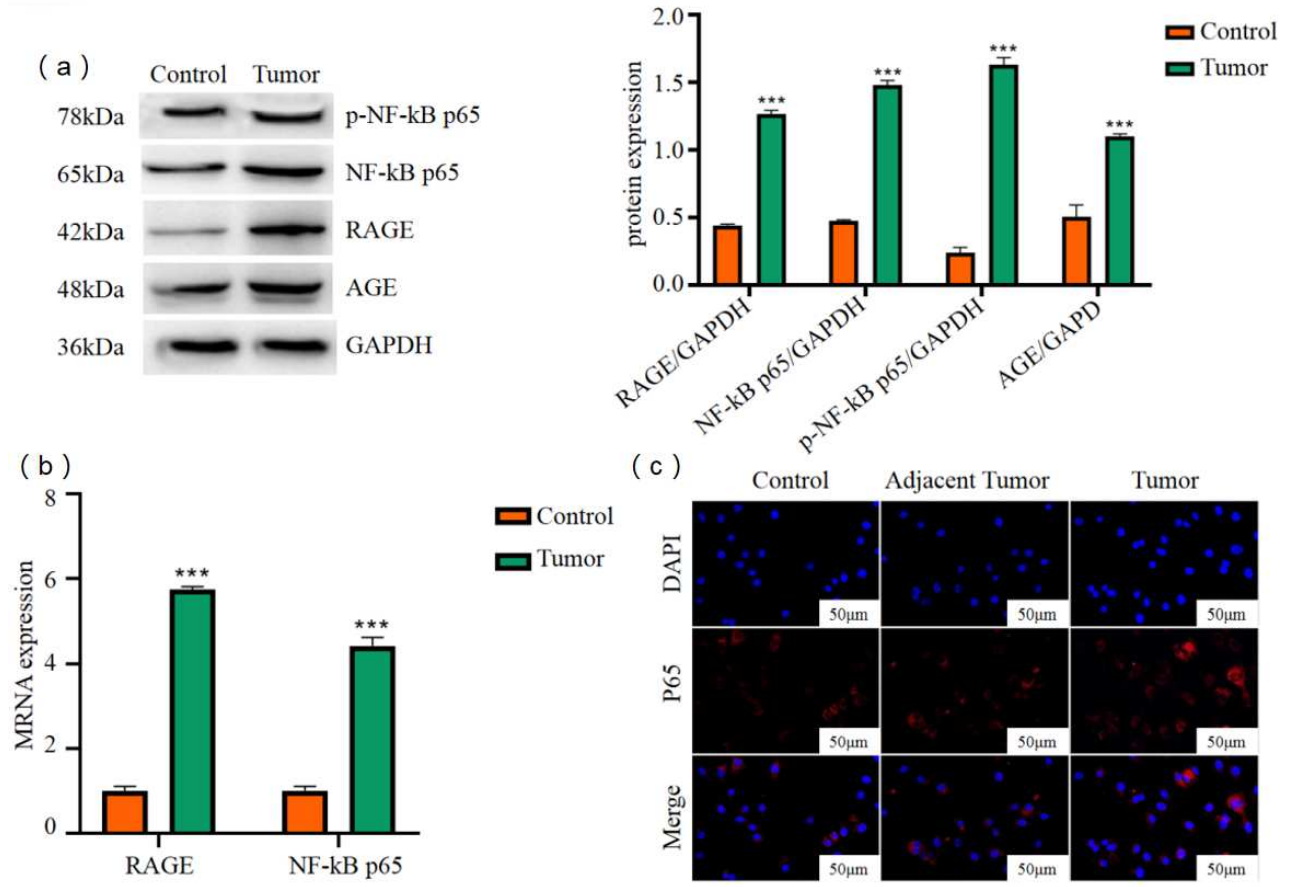

Fig. 1: AGEs/RAGE/NF-κB expression in oral squamous cell carcinoma.
(a) Western blot analysis of AGEs, RAGE, p65 and pp65 protein expression in OSCC tumor tissues (T) and paired adjacent normal tissues (N). GAPDH served as the loading control; (b) Quantitative reverse transcription PCR (RT-qPCR) analysis of RAGE and p65 mRNA expression levels in OSCC tissues and normal tissues. GAPDH was used as an internal control; (c) Immunofluorescence staining of p65 in OSCC and normal tissues. Nuclei were counterstained with DAPI . Arrows indicate nuclear translocation of p65 in OSCC cells. Scale bar = 20 μm.
Note: Data are presented as mean ± SD (n = 3 independent experiments). ***p* < 0.001 vs. normal tissues.Abbreviations: AGEs, advanced glycation end products; RAGE, receptor for AGEs; NF- κ B, nuclear factor-kappa; B; OSCC, oral squamous cell carcinoma; GAPDH, glyceraldehyde-3-phosphate dehydrogenase; DAPI, 4',6-diamidino-2-phenylindole; pp65, phosphorylated p65.

RESULTS

Expression of AGEs/RAGE/NF-κB in oral squamous cell carcinoma

Western blot analysis revealed that, compared to paired adjacent normal tissues, the expression levels of AGEs, RAGE, p65 protein and pp65 were significantly elevated in OSCC tumor tissues (P <0.01), indicating sustained activation of the NF-κB pathway in OSCC (Fig. 1A). RT-qPCR results further confirmed a significant upregulation trend in RAGE and p65 mRNA levels in tumor tissues (P <0.01), consistent with the changes observed at the protein level (Fig. 1B). Immunofluorescence detection of p65 subcellular localization demonstrated strong nuclear accumulation of p65 in OSCC tumor tissues, whereas p65 was primarily distributed in the cytoplasm in adjacent normal tissues (Fig. 1C). This result directly indicates that in OSCC, the NF-κB p65 subunit is constitutively activated

and translocates to the nucleus, potentially driving the transcription of its downstream target genes.

Knockdown of RAGE specifically inhibits the activation of NF-κB p65

To verify the necessity of RAGE in NF-κB activation, we screened three RAGE-specific siRNAs in Tca8113 cells. qPCR and Western blot results showed that siRNA-2 exhibited the highest knockdown efficiency at both the mRNA and protein levels (Fig. 2A). Therefore, siRNA-2 was selected for subsequent RAGE knockdown experiments. Western blot analysis demonstrated that after RAGE knockdown, the phosphorylation levels of IKKα (p-IKKα) and downstream pp65 were significantly lower than those in the siRNA-Ctrl group (P <0.001). In contrast, the total protein levels of IKKα and p65 showed no significant changes (Fig. 2B). This indicates that RAGE knockdown specifically inhibits the activation cascade of the NF-κB pathway. RT-qPCR revealed that mRNA expression levels of the NF-κB target genes IL-6 and MMP9 were significantly reduced in the siRNA-RAGE group compared to the siRNA-Ctrl group (Fig. 2C). Immunofluorescence results showed that after RAGE knockdown, the proportion of nuclear-localized p65 in Tca8113 cells significantly decreased, with p65 primarily retained in the cytoplasm in most cells (Fig. 2D). IHC staining indicated that compared to the siRNA-Ctrl group, pp65 protein was almost completely absent in Tca8113 cells of the siRNA-RAGE group, confirming the antibody's specificity for the target protein (Fig. 2E). These results demonstrate that in OSCC cells, the activation of NF-κB is specifically dependent on RAGE signaling.

AGEs/RAGE/NF-κB regulates miR-142-5p to engage in the development of oral squamous cell carcinoma

Bioinformatics analysis predicted a conserved binding site for hsa-miR-142-5p within the 3'-UTR region of p65 (Fig. 3A). In OSCC tumor tissues, the expression level of miR-142-5p was significantly lower than that in adjacent normal tissues (P <0.01). It showed a strong negative correlation with p65 protein levels ($P < 0.001$) (Fig. 3B). Dual-luciferase reporter assays confirmed that, compared with the negative control group, co-transfection with the miR-142-5p mimic significantly suppressed the luciferase activity of the reporter vector containing the wild-type p65 3'-UTR ($P < 0.01$). At the same time, no significant effect was observed on the vector with a mutated binding site. This demonstrates that p65 is a direct target of miR-142-5p (Fig. 3C).

3-Hydroxyflavone mediates the activation of NF-κB by miR-142-5p

To evaluate the direct impact of 3-Hydroxyflavone on OSCC cells, we assessed cell viability using the MTT assay. The results show that treatment with an effective concentration of 3-Hydroxyflavone significantly inhibited the proliferation and colony formation of Tca8113 cells compared to the control group (Control) ($P < 0.05$). This indicates that 3-Hydroxyflavone exerts a direct anti-proliferative effect on OSCC cells (Figs. 4A, 4B). To investigate the underlying mechanism of 3-Hydroxyflavone, we first validated the function of miR-142-5p. Western blot analysis showed that transfection of miR-142-5p mimic into OSCC cells significantly reduced the protein levels of RAGE and pp65 (P <0.05) (Fig. 4C). Immunofluorescence results further confirmed that overexpression of miR-142-5p effectively inhibited the nuclear translocation of p65 (Fig. 4D), suggesting that miR-142-5p suppresses the activation of downstream NF-κB p65 by targeting RAGE. We further linked the function of 3-Hydroxyflavone to miR-142-5p. Results demonstrated that both the miR-142-5p mimic and Flavonol groups significantly inhibited RAGE expression and p65 phosphorylation compared with the Control group, with the Flavonol group showing a more pronounced inhibitory effect ($P < 0.05$). Compared to the miR-142-5p mimic and Flavonol groups, the Flavonol + anti-miR-142-5p group partially reversed the inhibitory effect of 3-Hydroxyflavone on the RAGE/NF-κB pathway (Fig. 4E). This suggests that the inhibitory effect of 3-Hydroxyflavone on the RAGE/NF-κB pathway primarily depends on the upregulation of miR-142-5p.

Histological changes of oral squamous cell carcinoma and the expression of NF-κB are related to clinical outcomes

Immunohistochemical staining was performed on tumor tissues from 83 OSCC patients who received adjuvant therapy containing 3-Hydroxyflavone to analyze p65 protein expression. Based on staining scores, patients were divided into a p65 low-expression group (67 cases, 80.7%) and a p65 high-expression group (16 cases, 19.3%) (Fig. 5A). The clinicopathological characteristics of all patients are summarized in table 2, with no significant differences observed between the two groups in terms of age, gender, tumor stage, etc. (all P >0.05). All patients were followed up for 80 months, with a median follow-up time of (65.37 ± 12.63) months. Kaplan-Meier survival curves were plotted, and log-rank tests revealed that the overall survival rate at 80 months was higher in the p65 low-expression group (88.06%, 59/67) than in the p65 high-expression group (43.75%, 7/16) (Fig. 5B, $P < 0.01$). This suggests that 3-Hydroxyflavone treatment-induced inhibition of intratumoral p65 signaling may be associated with improved patient prognosis.

DISCUSSION

This study systematically elucidates, for the first time, the molecular mechanism underlying 3-Hydroxyflavone-mediated inhibition of OSCC cell proliferation and improvement of patient prognosis through modulation of the miR-142-5p/AGEs/RAGE/NF-κB signaling axis.

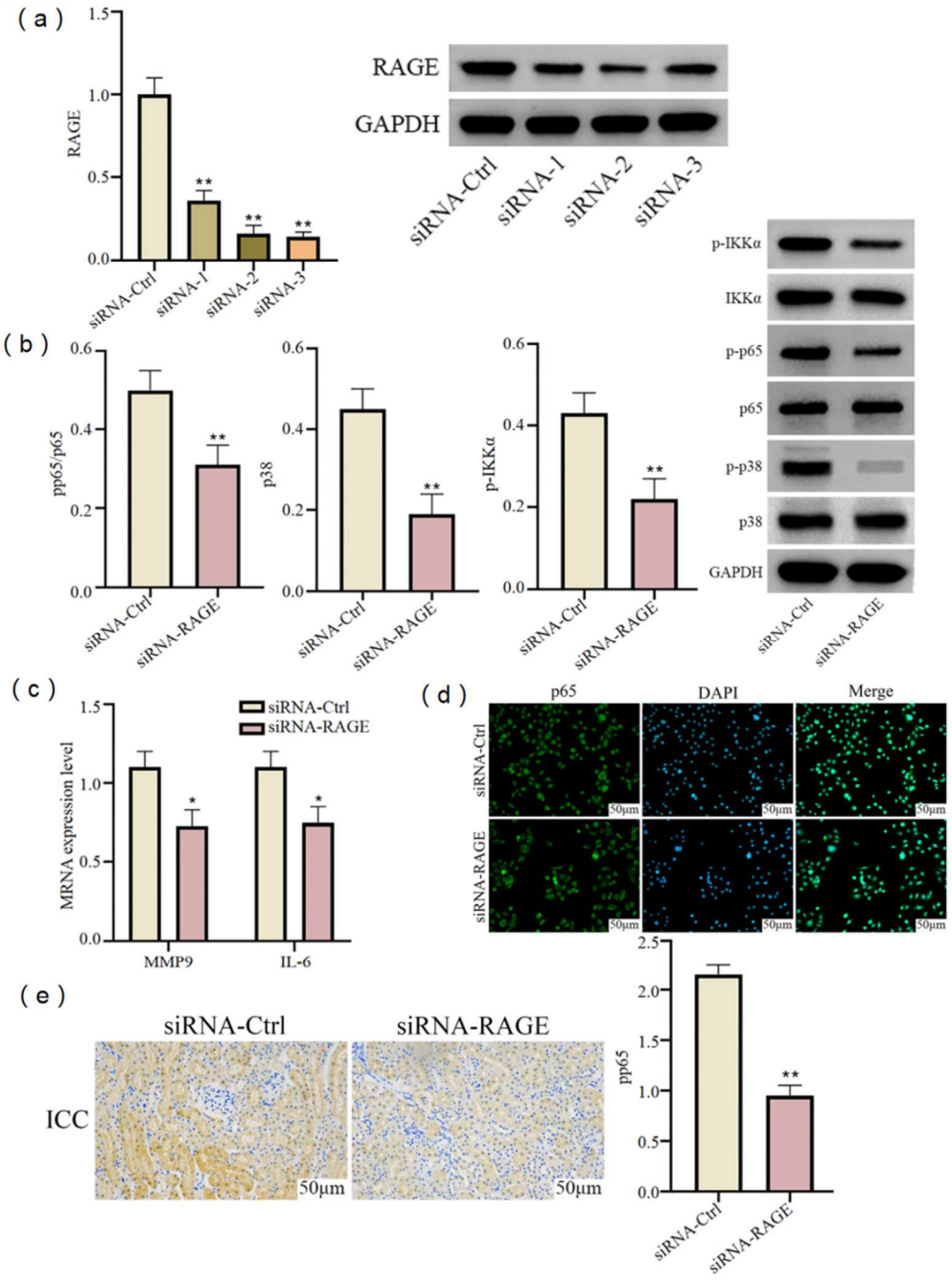

Fig. 2: Knockdown of RAGE specifically inhibits the activation of NF-κB p65.
(a) Screening of three RAGE-specific siRNAs (siRNA-1, siRNA-2, siRNA-3) by Western blot and RT-qPCR. siRNA-2 showed the highest knockdown efficiency and was selected for subsequent experiments; (b) Western blot analysis of p-IKKα, IKKα, pp65, and total p65 protein levels after RAGE knockdown. Quantification of protein bands is shown on the right. ***p* < 0.001 vs. siRNA-Ctrl group; (c) RT-qPCR analysis of NF-κB target genes IL-6 and MMP9 mRNA expression after RAGE knockdown. **p* < 0.01 vs. siRNA-Ctrl group; (d) Immunofluorescence staining showing p65 subcellular localization (green) after RAGE knockdown. Nuclei were stained with DAPI (blue). Arrows indicate nuclear p65. Scale bar = 20 μm; (e) Immunohistochemical (IHC) staining of pp65 in Tca8113 cells after RAGE knockdown. Scale bar = 50 μm.
Note: Data are presented as mean ± SD (n = 3 independent experiments). **p* < 0.01, ***p* < 0.001. Abbreviations: RAGE, receptor for AGEs; NF-κB, nuclear factor-kappa B; siRNA, small interfering RNA; IKKα, IκB kinase alpha; p-IKKα, phosphorylated IKKα; pp65, phosphorylated p65; IL-6, interleukin-6; MMP9, matrix metalloproteinase-9; Ctrl, control; DAPI, 4',6-diamidino-2-phenylindole; IHC, immunohistochemistry.

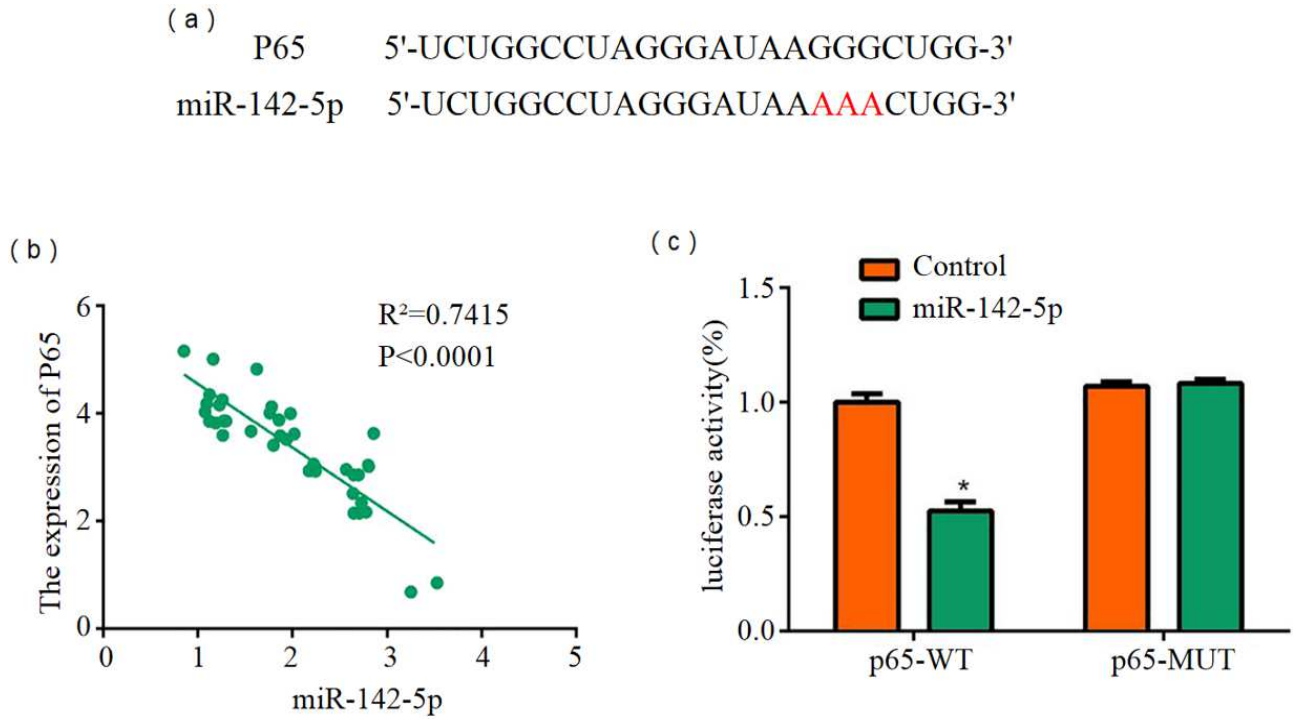

Fig. 3: The AGEs/RAGE/NF-κB pathway participates in the development of oral squamous cell carcinoma via miR-142-5p. (a) TargetScan bioinformatics prediction showing the conserved binding site of hsa-miR-142-5p within the 3'-untranslated region (3'-UTR) of p65 mRNA. The mutated sequence used for the luciferase assay is shown below; (b) Relative expression of miR-142-5p in OSCC tumor tissues (T) compared to adjacent normal tissues (N) measured by RT-qPCR. The lower panel shows a negative correlation between miR-142-5p expression and p65 protein levels (Pearson correlation analysis); (c) Dual-luciferase reporter assay. Tca8113 cells were co-transfected with a luciferase reporter vector containing either the wild-type (WT) or mutated (MUT) p65 3'-UTR, together with either miR-142-5p mimic or negative control miRNA (miR-Ctrl). Firefly luciferase activity was normalized to Renilla luciferase activity. **p* < 0.01 vs. miR-Ctrl group.

Note: Data are presented as mean ± SD (n = 3 independent experiments). **p* < 0.01, ***p* < 0.001. Abbreviations: AGEs, advanced glycation end products; RAGE, receptor for AGEs; NF-κB, nuclear factor-kappa B; OSCC, oral squamous cell carcinoma; UTR, untranslated region; RT-qPCR, reverse transcription quantitative polymerase chain reaction; WT, wild-type; MUT, mutated; ns, not significant.

Our findings not only highlight the critical role of this pathway in OSCC pathogenesis but also establish 3-Hydroxyflavone as a natural bioactive compound that exerts antitumor effects by specifically targeting this regulatory axis.

Our data confirm constitutive activation of the AGEs/RAGE/NF-κB pathway in OSCC. Compared with adjacent normal tissues, OSCC specimens exhibited significantly elevated expression of AGEs, RAGE and phosphorylated p65 (p-p65), along with pronounced nuclear translocation of p65. These observations align with reports in other solid malignancies, including pancreatic and prostate cancers, indicating that aberrant activation of this pathway critically contributes to OSCC progression (Senavirathna *et al*., 2023; Khoo *et al*., 2023). By specifically knocking down RAGE, we further demonstrated that NF-κB p65 activation is dependent on RAGE signaling. Concurrently, the expression of downstream pro-inflammatory factors such as IL-6 and Matrix Metalloproteinase-9 (MMP-9) was also suppressed. This indicates that RAGE serves as a critical upstream node regulating NF-κB activation in OSCC, thereby inhibiting tumor cell proliferation and invasive capacity.

Furthermore, miR-142-5p-mediated programmed death-ligand 1 (PD-L1) expression may contribute to immune evasion. The programmed cell death protein 1 (PD-1)/PD-L1 axis functions as an immune checkpoint, enabling PD-L1-expressing cells to escape immune surveillance (Zhang *et al*., 2025). Additionally, abnormal p65 expression in cancer cells may disrupt antitumor immune responses, protecting cells from T cell-mediated cytotoxicity (Bao *et al*., 2023). Our study revealed significant downregulation of miR-142-5p expression in OSCC tissues, which correlated negatively with p65 protein levels. Bioinformatics predictions and dual-luciferase reporter assays confirmed that p65 is a direct target of miR-142-5p.

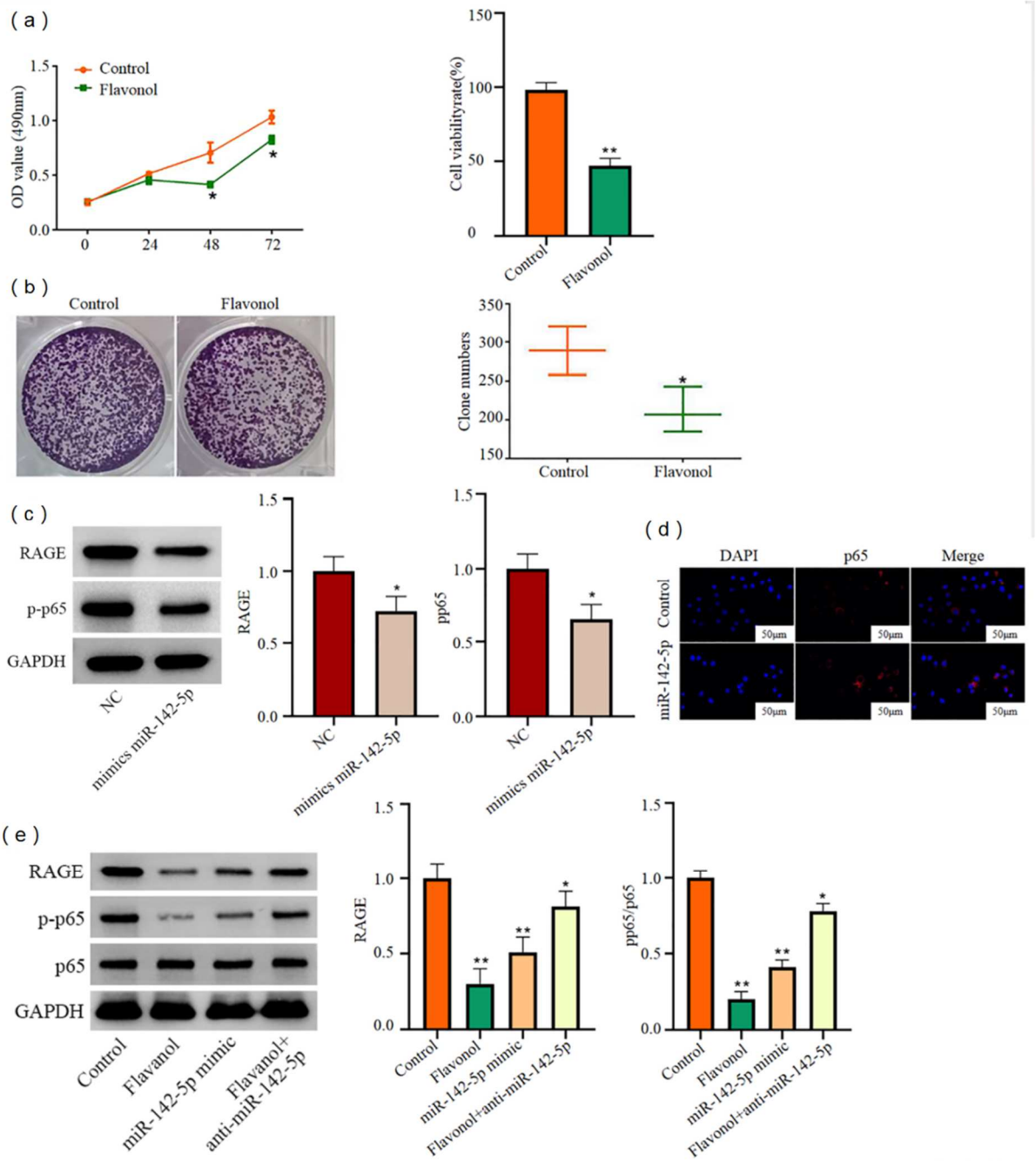

Fig. 4: 3-Hydroxyflavone mediates the activation of NF-κB by miR-142-5p.
(a) MTT assay showing cell viability of Tca8113 cells treated with 20 μM 3-Hydroxyflavone (Flavonol) or DMSO vehicle (Control) for 24, 48, and 72 hours. *p* < 0.05, **p* < 0.01 vs. Control; (b) Colony formation assay. Representative images and quantification of Tca8113 cell colonies after 14 days of treatment with 3-Hydroxyflavone or DMSO. **p* < 0.01 vs. Control; (c) Western blot analysis of RAGE, p65, and pp65 protein expression in Tca8113 cells transfected with miR-142-5p mimic or negative control miRNA (miR-Ctrl). GAPDH served as the loading control. **p* < 0.01 vs. miR-Ctrl; (d) Immunofluorescence staining of pp65 in Tca8113 cells after miR-142-5p mimic transfection. Nuclei were stained with DAPI. Scale bar = 20 μm; (e) Western blot analysis comparing RAGE and pp65/p65 protein levels across four groups: Control (DMSO), miR-142-5p mimic, Flavonol (20 μM 3-Hydroxyflavone), and Flavonol + anti-miR-142-5p. Quantification is shown on the right. *p* < 0.05, **p* < 0.01.
Note: Data are presented as mean ± SD (n = 3 independent experiments). *p* < 0.05, **p* < 0.01. Abbreviations: NF-κB, nuclear factor-kappa B; RAGE, receptor for AGEs; pp65, phosphorylated p65; DMSO, dimethyl sulfoxide; GAPDH, glyceraldehyde-3-phosphate dehydrogenase; anti-miR, antisense inhibitor of miR-142-5p.

Table 2: Clinicopathological characteristics of patients with oral squamous cell carcinoma and their association with p65 expression

Indicator		Total cases (n=83)	p65 High expression group (n=16)	p65 Low expression group (n=67)	t/χ2/Z	P
Gender [n(%)]	Male	45(54.22)	9(56.25)	36(53.73)	0.033	0.856
	Female	38(45.78)	7(43.75)	31(46.27)		
Age [n(%)]	< 60 years	56(67.47)	10(62.50)	46(68.66)	0.223	0.637
	⩾ 60 years	27(32.53)	6(37.50)	21(31.34)		
Histological Grade [n(%)]	I	27(32.53)	7(43.75)	20(29.85)	1.137	0.286
	II~III	56(67.47)	9(56.25)	47(70.15)		
BMI [n(%)]	18.5~24.0kg/m2	50(60.24)	10(62.50)	40(59.70)	0.199	0.843
	<18.5kg/m2	11(13.25)	2(12.50)	9(13.43)		
	⩾24.0kg/m2	22(26.51)	4(25.00)	18(26.87)		
Smoking History [n(%)]	No	60(72.29)	11(68.75)	49(73.13)	0.002	0.967
	Yes	23(27.71)	5(31.25)	18(26.87)		
Alcohol History [n(%)]	No	67(80.72)	13(81.25)	54(80.60)	0.086	0.769
	Yes	16(19.28)	3(18.75)	13(19.40)		
Primary Site [n(%)]	Tongue	33(39.76)	6(37.50)	27(40.30)	0.145	0.885
	Buccal	20(24.10)	4(25.00)	16(23.88)		
	Gingiva	14(16.87)	3(18.75)	11(16.42)		
	Other	16(19.28)	3(18.75)	13(19.40)		
Treatment Modality [n(%)]	Surgery only	46(55.42)	9(56.25)	37(55.22)	0.102	0.919
	Surgery+Chemotherapy	10(12.05)	2(12.50)	8(11.94)		
	Surgery+Radiotherapy	16(19.28)	3(18.75)	13(19.40)		
	Surgery+Chemoradiotherapy	11(13.25)	2(12.50)	9(13.43)		
TNM Stage [n(%)]	I+II	53(63.86)	12(75.00)	41(61.19)	1.067	0.302
	III+Ⅳ	30(36.14)	4(25.00)	26(38.81)		

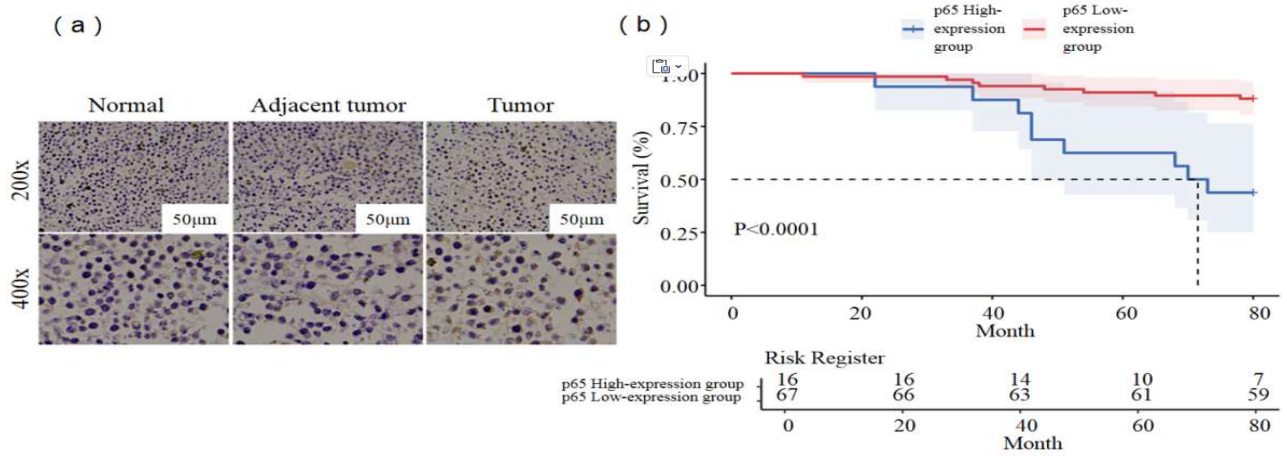

Fig. 5: 3-Hydroxyflavone-mediated histological changes in oral squamous cell carcinoma are associated with NF-κB expression and unfavorable clinical outcomes.

(a) Representative immunohistochemical (IHC) staining of p65 in OSCC tumor tissues from patients with low p65 expression (left) and high p65 expression (right). Scale bar = 100 μm. Based on staining scores, 67 patients (80.7%) were classified into the p65 low-expression group and 16 patients (19.3%) into the p65 high-expression group; (b) Kaplan-Meier survival curves showing overall survival of OSCC patients stratified by p65 expression level. The log-rank test was used for comparison. The 80-month overall survival rate was 88.06% (59/67) in the p65 low-expression group and 43.75% (7/16) in the p65 high-expression group.

Note: **p* < 0.01. Abbreviations: OSCC, oral squamous cell carcinoma; IHC, immunohistochemistry.

These findings indicate that reduced miR-142-5p expression in OSCC diminishes its inhibitory effect on p65, thereby alleviating negative regulation of the AGEs/RAGE/NF-κB pathway and promoting tumor progression. This observation aligns with previous studies reporting that miR-142-5p functions as a tumor suppressor in various cancers (Zareifar *et al*., 2024). Further mechanistic analysis revealed that in OSCC, the tumor suppressor miR-142-5p directly binds to the 3'-untranslated region (3'-UTR) of the mRNA encoding the NF-κB subunit p65, inhibiting its translation and establishing physiological negative regulation of the NF-κB pathway. When miR-142-5p expression is deficient, p65 protein levels become abnormally elevated, significantly enhancing cellular sensitivity to ligands such as AGEs within the tumor microenvironment. These ligands then activate NF-κB signaling via the RAGE receptor, ultimately leading to overexpression of downstream pro-oncogenic genes, including IL-6 and MMP-9 and directly driving aggressive tumor progression.

In addition to miR-142-5p activity, in p65-associated gastric cancer, miR-142-5p upregulation may occur through various mechanisms, including PD-L1 amplification and mutations in the PD-L1 3'-UTR (Shan *et al*., 2025). Furthermore, histologically, AGEs/RAGE/NF-κB-related gastric cancer is characterized by substantial lymphocyte infiltration and CD8+ cell secretion. Interferon-γ secreted by CD8+ cells induces signal transducer and activator of transcription 3 (STAT3) upregulation on cancer cells (Rojas *et al*., 2023; Lin *et al*., 2023). Notably, 3-Hydroxyflavone induces stem cell-like properties in cutaneous squamous cell carcinoma, whereas 3-Hydroxyflavone inhibition activates CD4+ T cells in patients with systemic lupus erythematosus (Koushki *et al*., 2024; Shen *et al*., 2021; Cheng *et al*., 2026). Most studies on 3-Hydroxyflavone have focused on its role in substrate modification, specifically its ability to act as an E3 ligase and influence small ubiquitin-related modifications (SUMOs) of transcription factors. In contrast, the present study reveals a distinct mechanism. Our study found that 3-Hydroxyflavone significantly inhibits RAGE expression and p65 phosphorylation in OSCC, with effects exceeding those of miR-142-5p mimics alone. When miR-142-5p function was partially blocked using an anti-miR-142-5p antagonist, the inhibitory effect of 3-Hydroxyflavone on the NF-κB pathway was markedly attenuated. These results indicate that the anti-OSCC activity of 3-Hydroxyflavone primarily depends on its ability to upregulate miR-142-5p, thereby suppressing the AGEs/RAGE/NF-κB signaling pathway and playing a crucial role in OSCC. The 3-Hydroxyflavone-mediated AGEs/RAGE/NF-κB axis contributes to OSCC pathogenesis by inducing signaling activation. miR-142-5p regulates NF-κB protein levels and affects p65 expression. p65, in turn, influences phosphorylation and modulates protein expression through DNA-binding activities (Xu *et al*., 2022). Phosphorylated p65 (pp65) functions through signal transduction to the nucleus (Sharen *et al*., 2022), regulating numerous genes and potentially inducing CD4+ T helper 17 (Th17) cell differentiation. Therefore, the "p65 downregulation/PD-L1 upregulation" axis may be important for both innate and adaptive immune regulation (Xu *et al*., 2026). The clinical relevance of this mechanism was validated in our patient cohort. Analysis of OSCC patients receiving adjuvant therapy containing 3-Hydroxyflavone revealed that those with low tumor p65 expression had significantly better overall survival than those with high p65 expression. These findings provide a translational foundation for 3-Hydroxyflavone-based therapeutic applications.

However, several limitations of this study should be acknowledged. First, our experiments were conducted primarily in OSCC cell lines. Although we adjusted the amount of transfected miR-142-5p mimics to approximate physiological expression levels and minimize transfection stress, stable transfection approaches yielded relatively low miR-142-5p expression compared with established cell models (Dai *et al*., 2025). Second, the association between p65 expression and survival outcomes suggests that p65 regulation may be influenced by both cancer cell-intrinsic factors and microenvironmental components.

CONCLUSION

In summary, 3-Hydroxyflavone inhibits tumor cell proliferation and improves patient prognosis by upregulating miR-142-5p, which suppresses the AGEs/RAGE/NF-κB signaling pathway, offering a novel strategy for OSCC treatment. Although this study primarily elucidates the mechanism at the cellular level, further validation of its in vivo efficacy and safety in animal models is still required. Future research should also delve deeper into the roles of the tumor microenvironment, AGE metabolism, and other 3-Hydroxyflavone structural analogs within this pathway to advance this discovery toward preclinical and clinical translation, ultimately providing new strategies for optimizing comprehensive OSCC treatment.

Acknowledgments
We gratefully acknowledge the Affiliated Yantai Yuhuangding Hospital of Qingdao University Laboratory for providing the necessary equipment for this study.

Authors' contributions
Yuan Cong: Conceived the research idea, designed the experimental plan, performed cell experiments and molecular assays, conducted data statistics and analysis, drafted the initial manuscript and prepared the figures; Shengzhi Wang: Supervised the research direction, provided clinical samples and resources, oversaw the experimental process, validated data results, revised and reviewed the manuscript and acquired research funding.

Funding
This research received no external funding.

Data availability statement
The datasets generated and/or analyzed during the current study are available from the corresponding author upon reasonable request.

Ethical approval
This study was approved by the Ethics Committee of The Affiliated Yantai Yuhuangding Hospital of Qingdao University (Approval Number: QD2025089). This study was performed in adherence with the STROBE guidelines. See supplementary file for the STROBE checklist.

Conflict of interest
The authors declare that this study was conducted in the absence of any commercial or financial relationships that could be construed as a potential conflict of interest.

Supplementary data
https://www.pjps.pk/uploads/2026/06/SUP1781769273.pdf

REFERENCES

Ai Y, Liu S, Luo H, Wu S, Wei H, Tang Z, Li X, Lv X and Zou C (2021). METTL3 intensifies the progress of oral squamous cell carcinoma via modulating the m6A amount of PRMT5 and PD-L1. *J Immunol Res*., **2021**:6149558.

Ayoolu OS, Ogbole OO, Ajaiyeoba EO, Nchiozem-Ngnitedem VA, Demissie TB, Elbadawi M, Efferth T, Bedane KG and Spiteller M (2022). Flavanols from *Tetrapleura tetraptera* with cytotoxic activities. *Fitoterapia*., **160**: 105206.

Bao Y, Zhai J, Chen H, Wong CC, Liang C, Ding Y, Huang D, Gou H, Chen D, Pan Y, Kang W, To KF and Yu J (2023). Targeting m6A reader YTHDF1 augments antitumour immunity and boosts anti-PD-1 efficacy in colorectal cancer. *Gut*., **72**(8): 1497–1509.

Cheng L, Tang Z, Li M and Huang C (2026). Hyperoside ameliorates lupus nephritis by suppressing AKT1-mediated PANoptosis in podocytes: Integrating network pharmacology and experimental validation. *Front Pharmacol*., **16**: 1726254.

Contrera KJ, Kansara S, Goyal N, Mady LJ, Puram SV, Young GD, Zandberg DP, Uppaluri R, Ferrarotto R, Holsinger FC, Ferris RL, Wenig BL and Curry JM (2025). Neoadjuvant therapy for mucosal head and neck squamous cell carcinoma: A review from the American head and neck society. *JAMA Otolaryngol Head Neck Surg*., **151**(6): 615–625.

Dai J, Wei H, Yang G and Zhao B (2025). miR-142-5p affects oral squamous cell carcinoma by regulating PIAS3/pSTAT3. *Ann Clin Lab Sci*., **55**(2): 179–184.

Dong H, Zhang Y, Huang Y and Deng H (2022). Pathophysiology of RAGE in inflammatory diseases. *Front Immunol*., **13**: 931473.

Feng J, Li S, Zhang B, Duan N, Zhou R, Yan S, Elango J, Liu N and Wu W (2022). FGFC1 exhibits anti-cancer activity via inhibiting NF-κB signaling pathway in EGFR-Mutant NSCLC cells. *Mar Drugs*., **20**(1): 76.

Gan X, Shu Z, Wang X, Yan D, Li J, Ofaim S, Albert R, Li X, Liu B, Zhou X and Barabasi AL (2023). Network medicine framework reveals generic herb-symptom effectiveness of traditional Chinese medicine. *Sci Adv*., **9**(43): eadh0215.

Hong SH, Kang N, Kim O, Hong SA, Park J, Kim J, Lee MA and Kang J (2022). EGFR-tyrosine kinase inhibitors induced activation of the autocrine CXCL10/CXCR3 pathway through crosstalk between the tumor and the microenvironment in EGFR-mutant lung cancer. *Cancers (Basel)*., **15**(1): 124.

Keam B, Machiels JP, Kim HR, Licitra L, Golusinski W, Gregoire V, Lee YG, Belka C, Guo Y, Rajappa SJ, Tahara M, Azrif M, Ang MK, Yang MH, Wang CH, Ng QS, Wan Zamaniah WI, Kiyota N, Babu S, Yang K and Pentheroudakis G (2021). Pan-asian adaptation of the EHNS-ESMO-ESTRO clinical practice guidelines for the diagnosis, treatment and follow-up of patients with squamous cell carcinoma of the head and neck. *ESMO Open*., **6**(6): 100309.

Khoo SH, Wu PR, Yeh KT, Hsu SL and Wu CH (2023). Biological and clinical significance of the AGE-RAGE axis in the aggressiveness and prognosis of prostate cancer. *J Food Drug Anal*., **31**(4): 664–682.

Koushki M, Amiri-Dashatan N, Rezaei-Tavirani M, Robati RM, Fateminasab F, Rahimi S, Razzaghi Z and Farahani M (2024). Screening the critical protein subnetwork to delineate potential mechanisms and protective agents associated with arsenic-induced cutaneous squamous cell carcinoma: A toxicogenomic study. *Food Chem Toxicol*., **185**: 114451.

Li X, Wang G, Sun X, Feng Y, Wang L, Sun G and Qiao H (2023). Effect of AGEs-RAGE system on the efficacy of PD-1 inhibitors in the treatment of driver-gene mutation negative advanced non-squamous non-small cell lung cancer. *Cell Mol Biol (Noisy-le-grand)*., **69**(14): 155–160.

Li X, Su Y, Li N, Zhang FR and Zhang N (2021). Berberine attenuates MPP+-induced neuronal injury by regulating LINC00943/miR-142-5p/KPNA4/NF-κB pathway in SK-N-SH cells. *Neurochem Res*., **46**(12): 3286–3300.

Li Z (2022). Overexpression of lncRNA HOXA-AS2 promotes the progression of oral squamous cell carcinoma by mediating SNX5 expression. *BMC Mol Cell Biol*., **23**(1):59.

Lin W, Luo Y, Wu J, Zhang H, Jin G, Guo C, Zhou H, Liang H and Xu X (2023). Loss of ADAR1 in macrophages in combination with interferon gamma suppresses tumor growth by remodeling the tumor microenvironment. *J Immunother Cancer*., **11**(11): e007402.

Lin Z, Chen M, Wan Y, Lei L and Ruan H (2020). miR-574-5p targets FOXN3 to regulate the invasion of

nasopharyngeal carcinoma cells via Wnt/β-Catenin pathway. *Technol Cancer Res Treat*., **19**: 1533033820971659.

Liu Y, Yang J, Weng D and Xie Y (2024). A1CF binding to the p65 interaction site on NKRF decreased IFN-β expression and p65 phosphorylation (Ser536) in renal carcinoma cells. *Int J Mol Sci*., **25**(7): 3576.

Pai S, Yadav VK, Kuo KT, Pikatan NW, Lin CS, Chien MH, Lee WH, Hsiao M, Chiu SC, Yeh CT and Tsai JT (2021). PDK1 inhibitor BX795 improves cisplatin and radio-efficacy in oral squamous cell carcinoma by downregulating the PDK1/CD47/Akt-mediated glycolysis signaling pathway. *Int J Mol Sci*., **22**(21):11492.

Pan S, Guan Y, Ma Y, Cui Q, Tang Z, Li J, Zu C, Zhang Y, Zhu L, Jiang J and Liu Z (2022). Advanced glycation end products correlate with breast cancer metastasis by activating RAGE/TLR4 signaling. *BMJ Open Diabetes Res Care*., **10**(2): e002697.

Rajesh RU and Sangeetha D (2024). Therapeutic potentials and targeting strategies of quercetin on cancer cells: Challenges and future prospects. *Phytomedicine*., **133**: 155902.

Rojas A, Lindner C, Schneider I, Gonzalez I and Morales MA (2023). Contributions of the receptor for advanced glycation end products axis activation in gastric cancer. *World J Gastroenterol*., **29**(6): 997–1010.

Senavirathna L, Pan S and Chen R (2023). Protein advanced glycation end products and their implications in pancreatic cancer. *Cancer Prev Res (Phila)*., **16**(11): 601–610.

Shan F, Shen S, Wang X and Chen G (2023). BST2 regulated by the transcription factor STAT1 can promote metastasis, invasion and proliferation of oral squamous cell carcinoma via the AKT/ERK1/2 signaling pathway. *Int J Oncol*., **62**(4):54.

Shan W, Li G, Zhang H, Zhang R, Liu J, Gao L, Li Y, Fan L, Yang C and Liu J (2025). TAP1 promotes immune escape by activating JNK/STAT1/PD-L1 signaling in EBV-associated gastric cancer. *Mol Cell Biochem*., **480**(10): 5429–5446.

Sharen G, Cheng H, Hu X, Miao J and Zhao D (2022). M1-like tumor-associated macrophages enhance proliferation and anti-apoptotic ability of liver cancer cells via activating the NF-κB signaling pathway. *Mol Med Rep*., **26**(5): 331.

Shen P, Lin W, Deng X, Ba X, Han L, Chen Z, Qin K, Huang Y and Tu S (2021). Potential implications of quercetin in autoimmune diseases. *Front Immunol*., **12**: 689044.

Tan Y, Wang Z, Xu M, Li B, Huang Z, Qin S, Nice EC, Tang J and Huang C (2023). Oral squamous cell carcinomas: State of the field and emerging directions. *Int J Oral Sci*., **15**(1): 44.

Tarle M and Luksic I (2024). Pathogenesis and therapy of oral carcinogenesis. *Int J Mol Sci*., **25**(12): 6343.

Xu B, Peng YJ and Zhu WJ (2022). Curcumin inhibits viability of clear cell renal cell carcinoma by down-regulating ADAMTS18 gene methylation though NF-κ B and AKT signaling pathway. *Chin J Integr Med*., **28**(5): 419–424.

Xu JZ, An Y, Sun JX, Xiong YF, Liu CQ, Zhang SH, Xia ZY, Hu J, Zhang ZY, Guo CX, Liu BL, Guan W, Wang SG and Xia QD (2026). Oncolytic virus OH2 induces PD-L1 upregulation via NF-κB signaling and synergizes with anti-PD-L1 therapy in prostate cancer through a targeted extracellular vesicle delivery system. *J Immunother Cancer*., **14**(2): e013818.

Zareifar P, Ahmed HM, Ghaderi P, Farahmand Y, Rahnama N, Esbati R, Moradi A, Yazdani O and Sadeghipour Y (2024). miR-142-3p/5p role in cancer: From epigenetic regulation to immunomodulation. *Cell Biochem Funct*., **42**(2): e3931.

Zhao W, Zheng XD, Tang PY, Li HM, Liu X, Zhong JJ and Tang YJ (2023). Advances of antitumor drug discovery in traditional Chinese medicine and natural active products by using multi-active components combination. *Med Res Rev*., **43**(5): 1778–1808.

Zhang Y, Liu C, Jin S, Xie L, Xiao Q and Yao J (2025). Ultrasound-targeted nanobubbles codelivering NKP-1339 and miR-142-5p for synergistic mitochondrial immunogenic cell death and PD-L1 inhibition in cancer therapy. *Biomater Res*., **29**: 0232.

Zou C, Lv X, Wei H, Wu S, Song J, Tang Z, Liu S, Li X and Ai Y (2022). Long non-coding RNA LINC00472 inhibits oral squamous cell carcinoma via miR-4311/GNG7 axis. *Bioengineered*., **13**(3):6371-6382.